Progress in Natural Science: Materials International 2012;22(1):15–20

Chinese Materials Research Society

Progress in Natural Science: Materials International

www.elsevier.com/locate/pnsmi
www.sciencedirect.com

ORIGINAL RESEARCH

# Fabrication of well-dispersive yttrium-stabilized cubic zirconia nanoparticles via vapor phase hydrolysis

**Fuzhi Shi[a], Yaogang Li[b], Hongzhi Wang[a], Qinghong Zhang[b,*]**

[a]*State Key Laboratory for Modification of Chemical Fibers and Polymer Materials, Donghua University, Shanghai 201620, China*
[b]*Engineering Research Centre of Advanced Glasses Manufacturing Technology, Donghua University, Shanghai 201620, China*

Received 15 October 2011; accepted 30 November 2011
Available online 9 February 2012

**KEYWORDS**

Cubic zirconia;
Yttrium-stabilized;
Vapor phase hydrolysis;
Layer by layer

**Abstract** The well-dispersive yttrium-stabilized cubic zirconia nanoparticles were fabricated via vapor phase hydrolysis process, and the as-synthesized cubic zirconia nanoparticles were characterized by X-ray diffraction (XRD), scanning electron microscopy (SEM), transmission electron microscopy (TEM), high-resolution electron microscopy (HRTEM) and $N_2$ adsorption–desorption isotherm analysis. The results of XRD indicated that the pure cubic zirconia nanocrystals were obtained with 8 mol% yttrium atoms doping. And SEM and TEM observation showed the yttrium-stabilized cubic zirconia nanoparticles (8 mol% yttrium) were dispersive well, with an average crystallite size of 5 nm. The zirconia coatings were fabricated via the layer by layer (LbL) assembly using poly (allylamine hydrochloride) as polyelectrolyte and cubic zirconia nanoparticles as building blocks in order to illustrate its good dispersity. The quartz substrate coated on both sides with 10 layers of yttrium-stabilized cubic zirconia nanoparticles exhibited transmittance as high as 92.3%, which was decreased only one percent compared with bare quartz substrate. Moreover, the stable super-hydrophilic wetting property of the coating was obtained after a critical number of layers (10 layers) deposited onto the surface of quartz substrate, due to its porous structures.



*Corresponding author. Tel.: +86 21 67792943; fax: +86 21 67792855.
E-mail address: zhangqh@dhu.edu.cn (Q. Zhang).



Peer review under responsibility of Chinese Materials Research Society.
doi:10.1016/j.pnsc.2011.12.003

**Production and hosting by Elsevier**

## 1. Introduction

Zirconia has received a great deal of attention owing to its application in a wide range of fields such as biomaterial ceramics [1,2], gas and humidity sensors [3–6], anode in fuel cells [7–9], catalysts [10–12] and opto-electrics [13]. These applications originate from the unique physical and chemical properties of $ZrO_2$, such as thermal stability, chemical resistance, mechanical characteristics and ionic conductivity [14]. It is well established that pure zirconia has three crystal structures and will undergo a succession of transformation from the

high-temperature high-symmetry cubic phase to slightly distorted structures with tetragonal and monoclinic symmetries [15]. The high-temperature cubic phase is very important because it is more valuable for the technological applications mentioned above than the room-temperature monoclinic and middle tetragonal phase. However, cubic $ZrO_2$ is unstable in bulk forms at ambient temperature [16]. Recently, lots of efforts were focused on preparation of stabilized cubic zirconia by importing different foreign elements, such as $Na^+$, $Y^{3+}$, $Ce^{4+}$ and $Ti^{4+}$ [17–20]. Yttrium is an effective stabilizer and is most widely used. Yang et al. [21] synthesized the yttria-doped $ZrO_2$ powders via solvothermal method. The particles had spherical morphology with an average crystallite size of 10 nm and agglomerated into bigger spheres with a diameter of about 120 nm.

Zirconia nanoparticles with different crystallite size and various surface morphologies have been obtained through different routes such as microwave plasma [22], spray pyrolysis [23], chemical vapor synthesis [24], non-hydrolytic sol–gel [25]. Nonetheless, most of zirconia nanoparticles fabricated by above mentioned method require subsequently heat treatment at high temperature, and then they will have poor dispersive property, broad particle size distribution, low specific surface area, high agglomeration, etc. The controllable synthetic procedure should be developed for the extensive applications of zirconia nanoparticles with highly crystalline and well dispersive property.

In this work, we reported a facile strategy to prepare well-dispersive yttrium-stabilized cubic zirconia (YSCZ) nanoparticles via vapor phase hydrolysis (VPH) of zirconium(IV) n-butoxide (ZBOT). The VPH method could not only control the hydrolysis of high reactivity metal alkoxide precursors, but also combine the water molecules gently contacting alkoxide in vapor form with the advantage of hydrothermal treatment to give highly-crystallized $ZrO_2$. The different crystal phase of $ZrO_2$ could be obtained through tuning the content of yttrium dopant. To the best of our knowledge, this is the first report on the synthesis well-dispersive cubic $ZrO_2$ nanocrystallites by this method. Finally, YSCZ thin coating was also fabricated via layer by layer assembly of YSCZ nanoparticles in order to illustrate the well dispersive property of zirconia nanoparticles, and an antifogging coating was obtained.

## 2. Experimental

### 2.1. Materials

Zirconium(IV) n-butoxide (ZBOT, 80%) was purchased from Aldrich. Yttrium nitrate hexahydrate and absolute ethanol were analytical grade, and purchased from Shanghai Chemical Regent Co., China. All chemicals were used as received without further purification. The deionized water for all treatment processes was purified by ion exchange and then followed by distillation.

### 2.2. Synthesis of well-dispersive YSCZ nanoparticles

The well-dispersive YSCZ nanoparticles were prepared by the vapor phase hydrolysis method [26,27], which was recently used to prepare core/shell structured photocatalysts. 1.5 mmol raw sources followed the $Y_xZr_{100-x}O_2$ ($x=0$, 3 and 8) composition were dissolved into 8 mL absolute ethanol and stirred for 2 min. Then the solution was transferred into the vapor phase hydrolysis device (VPHD) quickly. 3 mL deionized water was located at the bottom of VPHD as liquid phase to produce water vapor at elevated temperature. Thus the liquid water did not contact ZBOT directly and the fierce hydrolysis was avoided. The sealed VPHD was heated to 200 °C and held for 12 h. Then, the VPHD was cooled to ambient temperature. The as-synthesized powder was collected by centrifugation and rinsed with deionized water and absolute ethanol for three times, respectively. The $Y_8Zr_{92}O_2$ nanoparticles (8YSCZ) synthesized by vapor hydrolyzing ZBOT at 200 °C for 12 h were dispersed into absolute ethanol to obtain a colloidal zirconia suspension (0.15‰ w/w) for layer by layer assembling.

### 2.3. Fabrication of 8YSCZ coatings

Quartz substrates were cleaned via treatment with Pirahna solution (4:1:40 (v/v/v) mixture of 98% $H_2SO_4$, 30% $H_2O_2$ and deionized $H_2O$) at 80 °C for 20 min, rinsed with a copious amount of deionized water. *Caution! Piranha solution is highly corrosive. Extreme care should be taken when handling Piranha solution, and only small quantities should be prepared.* Then quartz substrates were further cleaned by treatment with another solution (4:1:40 (v/v/v) mixture of 28% $NH_3 \cdot H_2O$, 30% $H_2O_2$ and deionized $H_2O$) at 80 °C for 20 min. This treatment imparts negative charges on the substrate, allowing subsequent adsorption of polyelectrolyte (PAH).

Then multilayer coatings of poly(allylamine hydrochloride)/8YSCZ (PAH/8YSCZ) were deposited on the quartz substrates via layer by layer method according to the following general protocol: (i) the quartz substrates were rinsed with a copious amount of deionized water, and dipped into the ethanol suspension of 8YSCZ for 15 min, followed by rinsing with deionized water thoroughly; (ii) the quartz substrates were dipped into an aqueous solution of PAH (0.94‰ w/w) for 15 min and washed with deionized water. Subsequently, steps (i) and (ii) were repeated until the desired number of deposition cycles was reached. In order to remove PAH, the quartz substrate covered with PAH/8YSCZ multilayer coating was calcined in an oven at 500 °C for 4 h.

### 2.4. Characterization

The powder phase composition was identified by X-ray diffraction (XRD) equipment (D/max 2550 PC, Rigaku, Japan), using Cu Kα radiation at 40 kV and 200 mA. The crystallite size of $ZrO_2$ was estimated from the corresponding XRD peak at $2\theta = 30.1^\circ$ by Scherrer formula. The morphology and size of the powders were observed using transmission electron microscope (TEM) (JEM-2100F, JEOL, Japan) and high-resolution transmission electron microscopy (HRTEM) with an accelerating voltage 200 kV. Scanning electron microscopy (SEM) images were collected on scanning electron microscope (S-4800, Hatachi, Japan) equipped with an energy-dispersive X-ray (EDX). The nitrogen adsorption–desorption isotherm was obtained at 77 K using a Autosorb-1 MP (Quantachrome, USA) utilizing Barrett–Emmett–Teller (BET) calculations of specific surface area and density functional theory (DFT) calculations of pore volume and pore size (diameter) distributions from the adsorption branch of the isotherm. Sessile drop contact angle

measurements utilizing deionized water (>18 ΩM cm) were performed with a contact angle meter (Contact Angle System OCA40, Dataphysics Co., Germany). A water drop of approximately 3 μL was placed on the surfaces using a syringe. Transmittance spectra were recorded using PE Lambda 950 spectrophotometer (Perkin-Elmer Co., USA).

## 3. Results and discussion

The X-ray diffraction patterns of as-prepared zirconia nanoparticles synthesized at 200 °C with different yttrium content are shown in Fig. 1. As can be seen, both monoclinic (JCPDS No. 65-1024) and cubic (JCPDS No. 49-1642) $ZrO_2$ coexist in the resulted product when the yttrium is added not enough (curve a and b). The peaks of monoclinic phase decrease and weaken compared to pure zirconia (curve a) when doped 3 mol% yttrium atoms. And all X-ray diffraction peaks of curve c are comparable with the standard data of pure cubic $ZrO_2$. Although it is difficult to distinguish the tetragonal and cubic phase from XRD pattern, Lamas et al. [15,28] reported that the (4 0 0) peak of cubic zirconia did not split into two peaks, which was characteristic of the cubic phase but not tetragonal phase. XRD also suggests that 8 mol% yttrium dopant could stabilize $ZrO_2$ nanocrystal and make it be cubic phase in these experimental conditions, which is agreed with the result of Yang et al. [21]. It is clear that the broadening XRD peak indicates that the crystallite size of 8YSCZ is fine. The crystallite size calculated by Scherrer formula from the broadening (1 1 1) plane at $2\theta = 30.1^\circ$ is about 5.2 nm. Even if the yttrium content reached to 8 mol%, and there is no any peaks of $Y_2O_3$ can be observed. It means the yttrium atom has been doped into the zirconia lattice, indicating the phase purity of the synthesized $ZrO_2$ powders.

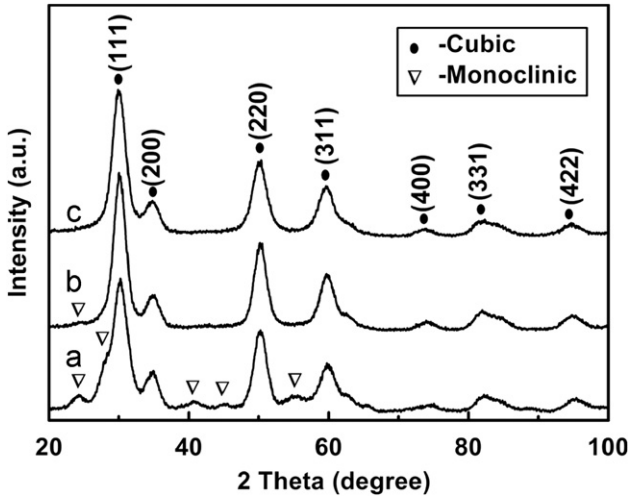


**Fig. 1** X-ray diffraction patterns of zirconia nanoparticles synthesized at 200 °C for 12 h with different yttrium content (a) 0 mol% (pure $ZrO_2$), (b) 3 mol% and (c) 8 mol% (8YSCZ).

The morphologies of zirconia nanoparticles synthesized at 200 °C with different yttrium content are revealed by scanning electron microscopy (SEM) as shown in Fig. 2. Fig. 2a shows that $ZrO_2$ crystallites aggregate into large particles ranged from several hundred nanometers to micrometers when there is no yttrium doped. Fig. 2b reveals that the 8YSCZ particles are very fine and the dispersive property of 8YSCZ powder is very well. A possible reason is that the yttrium incorporation influences the surface absorption energy, similar as the surface absorption energy can control the impurity doping [29]. $ZrO_2$ nanoparticles are not agglomerated. EDX displays the sample contains only C, O, Al, Zr elements when there is no yttrium

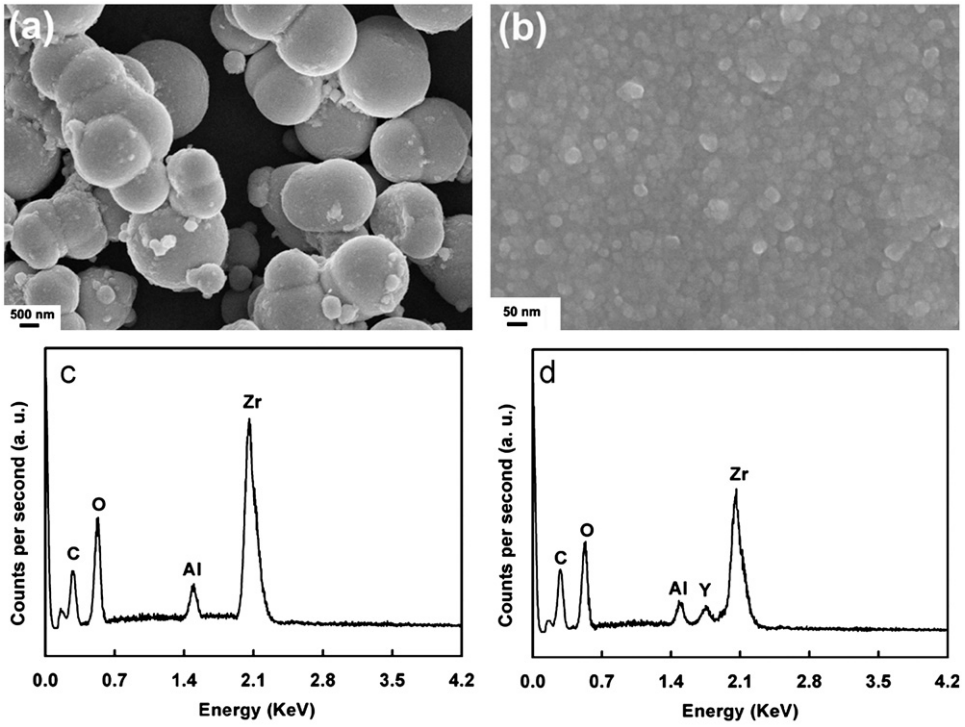


**Fig. 2** SEM images of (a) pure $ZrO_2$ (0 mol%), (b) 8 YSCZ and EDX of (c) pure $ZrO_2$ (0 mol%), (d) 8YSCZ.

doped, and C, O, Al, Y, Zr elements for 8YSCZ powders. C could be attributed to the carbon coating introduced during the sample preparation process, Al peak is caused by the supporting substrate of SEM sample and no other peaks belong to other impurities appear on the spectrum. Both the atomic ratios (Zr/O) of two samples are approximate 1:2, and the difference between Fig. 2c and d is only the peak of yttrium. SEM analysis indicates that the yttrium dopant plays a very crucial role in fabrication of well-dispersive zirconia nanoparticles.

A representative TEM image of 8YSCZ powders is shown in Fig. 3a, the well-dispersive $ZrO_2$ nanoparticles can be observed. Most of the zirconia nanoparticles have spherical morphologies and no highly aggregated particles can be observed. HRTEM image further supports the single-crystalline nature of the particles (Fig. 3b). The diameter of spherical nanocrystals is observed to be about 5 nm, which is consistent with that calculated from XRD data. The corresponding lattice spacings of 0.298 nm and 0.254 nm can be assigned to the (1 1 1) and (2 0 0) planes of cubic $ZrO_2$, respectively [13]. The selected area electron diffraction (SAED) pattern is shown in Fig. 3c. The diffraction rings also illustrate the crystalline nature of cubic $ZrO_2$. The well-dispersive cubic $ZrO_2$ with single and pure crystalline phase signify the importance of the present synthesis technique in obtaining cubic $ZrO_2$ nanoparticles with good dispersity, narrow size distribution, high purity and high crystallinity.

The $N_2$ adsorption–desorption isotherm (Fig. 4) of 8YSCZ powders appears to be a type IV-like curve with a hysteresis loop of type III, characteristic of the micro-pores and meso-pores exist in the sample. This could be attributed to the fine crystallite size and well dispersive nature. The specific surface area of 8YSCZ calculated by BET is 260 $m^2/g$ and greater than reported values using the hydrothermal or solvothermal method [30,31]. The mean diameter of 8YSCZ nanoparticles could also be calculated by specific surface area according to the following equations:

$$D = \frac{6}{S\rho} \tag{1}$$

in which $\rho$ is the crystalline density of cubic zirconia and equal to 5.6 $g/cm^3$, $D$ is the mean diameter of zirconia crystallites and $S$ means the specific surface area. The diameter calculated by formula (1) is about 4.1 nm, which is closed to the results of XRD and TEM.

It is common knowledge that the isoelectric point of $ZrO_2$ nanoparticles is in the range from pH = 4 to pH = 6. The external surface of $ZrO_2$ nanoparticles is negatively charged when pH > 6. Therefore, $ZrO_2$ nanoparticles can be used as building blocks without any surface modification for the assembly of functional coatings with positively charged electrolytes by the electrostatic layer by layer assembling. In this work, the negatively charged 8YSCZ nanoparticles were alternately deposited with positively charged PAH to fabricate PAH/8YSCZ multilayer coatings. The 8YSCZ coatings with different layers are obtained by calcination the coating at 500 °C for 4 h. This well-known calcination process burns out the polymer component of coatings and enhances the mechanical durability and adhesion of 8YSCZ coatings. This process is similar with the silica to form the stable siloxane bridges [32]. The transmission spectra of the selected samples in visible region are shown in Fig. 5. Compared with the transmittance of curve a (93.3%), the transmittance of curve b (ca. 92.3%) and c (91.7%) indicate the fact that the transmittance is decreasing with increasing the 8YSCZ layers. But the transmittance decrease only 1.8% even if coated 20 layers. The transmittance can ensure their applications in modern technology such as displays and optical filters. Fig. 5 (inset) shows the SEM image of quartz substrate covered with 10 layers of PAH/8YSCZ and 8YSCZ nanoparticles. The PAH/8YSCZ coating is relatively compact and some pores can be clearly observed on the surface of 8YSCZ coatings, and the pore size is less than one hundred nanometer. The morphological feature of the coating would be beneficial to enhance its super-hydrophilicity or transmittance [33–35].

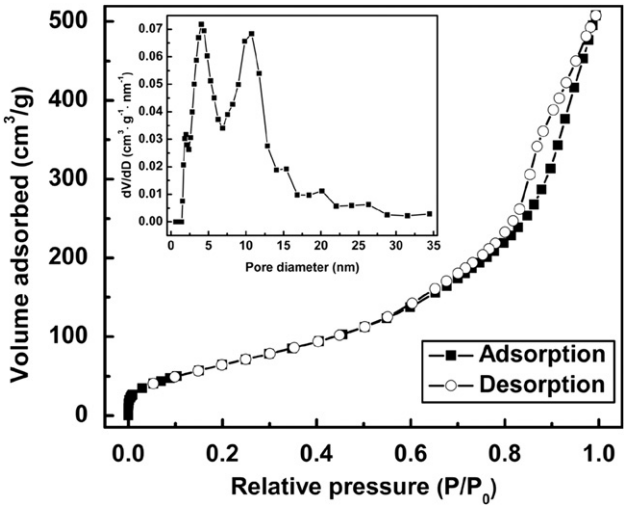


**Fig. 4** $N_2$ adsorption–desorption isotherm of 8YSCZ powders at 77 K with corresponding pore size distribution calculated by density functional theory (DFT) method from adsorption branch (inset).

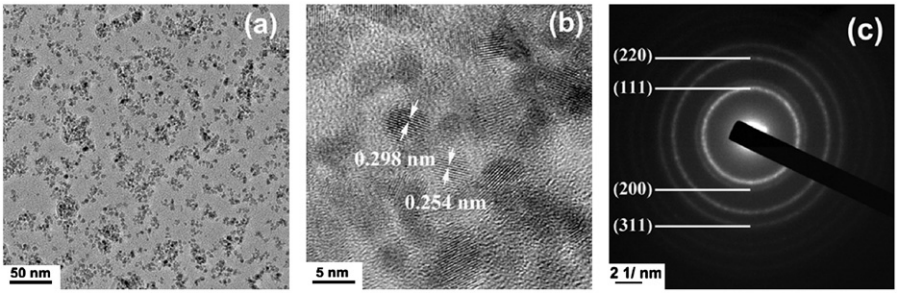


**Fig. 3** TEM, HRTEM and SAED images of 8YSCZ via vapor hydrolyzing ZBOT at 200 °C for 12 h.

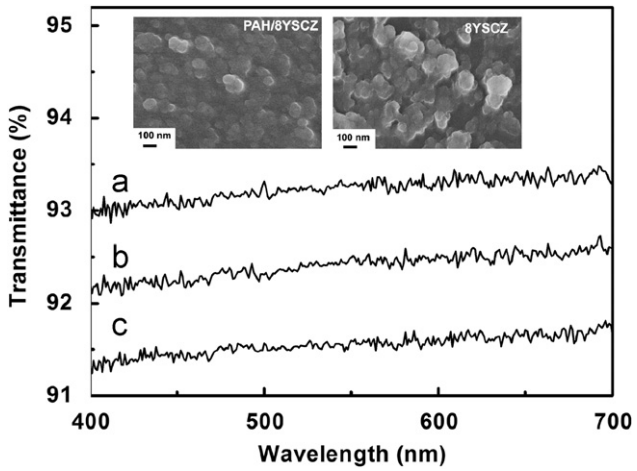


**Fig. 5** Transmission spectra of (a) bare quartz substrate; (b) quartz substrate covered with 10 layers of 8YSCZ nanoparticles; (c) quartz substrate covered with 20 layers of 8YSCZ nanoparticles; SEM image of quartz substrate covered with 10 layers of PAH/8YSCZ and 8YSCZ nanoparticles (inset).

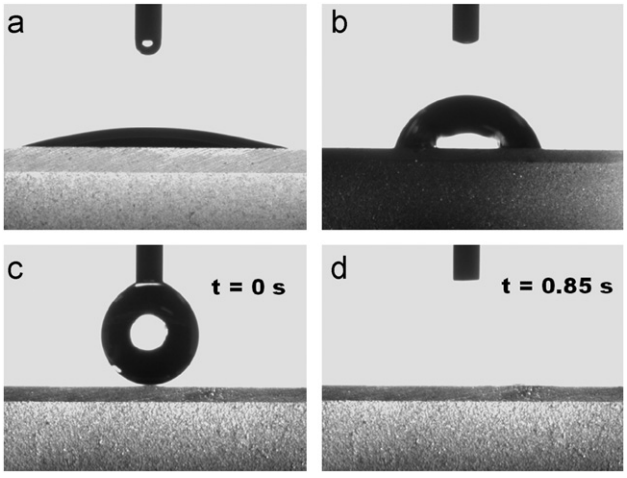


**Fig. 6** Still images from video contact angle measurements for a water droplet (3 μL) spreading on different samples. (a) Bare quartz substrate; (b) quartz substrate covered with 10 layers of PAH/8YSCZ coating; (c) 0 s and (d) 0.85 s of quartz substrate covered with 10 layers of 8YSCZ nanoparticles after calcined at 500 °C for 4 h.

Super-hydrophilic coatings can significantly suppress the fogging behavior because condensed water droplets will spread flatly almost instantaneously to form a thin sheet-like water membrane. In this way, light scattering by the condensed water droplets was eliminated. The super-hydrophilic properties of quartz substrate covered with 10 layers of 8YSCZ nanoparticles originate from its porous structure. The photographs (c and d) in Fig. 6 illustrate the antifogging behavior of 8YSCZ coating with 10 layers. The contact angle of a water droplet (3 μL) on 8YSCZ coating with 10 layers becomes about 0° in around 0.85 s. The contact angles of a water droplet (3 μL) on bare quartz substrate (Fig. 6a) and PAH/8YSCZ coating with 10 layers (Fig. 6b) are about 31.6° and 83.1°, respectively. So up to now, the superhydrophilic $ZrO_2$ coatings are certified by the quick response of 0.85 s from video contact angle measurements.

## 4. Conclusions

In summary, the well-dispersive yttrium-stabilized cubic $ZrO_2$ with single and pure crystalline phase has been prepared via vapor phase hydrolysis process. The characterization results signify the importance of the present synthesis technique in obtaining well-dispersive cubic $ZrO_2$ nanoparticles with a narrow size distribution, high purity and high crystallinity. The yttrium dopant plays a very crucial role in fabrication of well-dispersive cubic zirconia nanoparticles and the average crystallite of it is about 5 nm. The quartz substrate coated on both sides with 10 layers of yttrium-stabilized cubic zirconia nanoparticles exhibits high transmittance and superhydrophilic property due to its porous structures.

## Acknowledgments

Research was supported by the National Key Technology R&D Program (No. 2006BAA04B02-01), the National Natural Science Foundation of China (No. 50925312), Shanghai Leading Academic Discipline Project (B603), the Cultivation Fund of the Key Scientific and Technical Innovation Project (No. 708039) and the Program of Introducing Talents of Discipline to Universities (No. 111-2-04).

## References

[1] N. Beck, F. Graef, M. Wichmann, et al., In vitro fracture resistance of copy-milled zirconia ceramic posts, Journal of Prosthetic Dentistry 103 (1) (2010) 40–44.
[2] C. Piconi, G. Maccauro, Zirconia as a ceramic biomaterial, Biomaterials 20 (1) (1999) 1–25.
[3] V.V. Plashnitsa, P. Elumalai, Y. Fujio, et al., Zirconia-based electrochemical gas sensors using nano-structured sensing materials aiming at detection of automotive exhausts, Electrochimica Acta 54 (25) (2009) 6099–6106.
[4] I.C. Cosentino, E.N.S. Muccillo, R. Muccillo, Development of zirconia–titania porous ceramics for humidity sensors, Sensors and Actuators B 96 (3) (2003) 677–683.
[5] W.C. Maskell, Progress in the development of zirconia gas sensors, Solid State Ionics 134 (1–2) (2000) 43–50.
[6] J. Wang, M.Y. Su, J.Q. Qi, et al., Sensitivity and complex impedance of nanometer zirconia thick film humidity sensors, Sensors and Actuators B 139 (2) (2009) 418–424.
[7] H. Koide, Y. Someya, T. Yoshida, et al., Properties of Ni/YSZ cermet as anode for SOFC, Solid State Ionics 132 (3–4) (2000) 253–260.
[8] D. Yoon, J.J. Lee, H.G. Park, et al., NiO/YSZ–YSZ nanocomposite functional layer for high performance solid oxide fuel cell anodes, Journal of The Electrochemical Society 157 (4) (2010) B455–B462.
[9] Y. Mizutani, K. Hisada, K. Ukala, et al., From rare earth doped zirconia to 1 kW solid oxide fuel cell system, Journal of Alloys and Compounds 408 (2006) 518–524.
[10] F.T. Vieira, M.A.S. Baldanza, M. Schmal, Influence of oxygen and promoting effect of barium on the reduction of $NO_x$ by ethanol on $Pd/ZrO_2$ catalyst, Catalysis Today 149 (3-4) (2010) 304–308.
[11] W.P. Dow, Y.P. Wang, T.J. Huang, Yttria-stabilized zirconia supported copper oxide catalyst. 1. Effect of oxygen vacancy of support on copper oxide reduction, Journal of Catalysis 160 (2) (1996) 155–170.

[12] J. Kaspar, P. Fornasiero, Nanostructured materials for advanced automotive de-pollution catalysts, Journal of Solid State Chemistry 171 (1–2) (2003) 19–29.
[13] T.S. Wu, K.X. Wang, L.Y. Zou, et al., Effect of surface cations on photoelectric conversion property of nanosized zirconia, Journal of Physical Chemistry C 113 (21) (2009) 9114–9120.
[14] W. Wang, D. Weng, X.D. Wu, Preparation and thermal stability of zirconia-doped mullite fibers via sol–gel method, Progress in Natural Science 21 (2) (2011) 117–121.
[15] D.G. Lamas, A.M. Rosso, M.S. Anzorena, et al., Crystal structure of pure $ZrO_2$ nanopowders, Scripta Materialia 55 (6) (2006) 553–556.
[16] P. Manivasakan, V. Rajendran, P.R. Rauta, et al., Synthesis of monoclinic and cubic $ZrO_2$ nanoparticles from zircon, Journal of the American Ceramic Society 94 (5) (2011) 1410–1420.
[17] J. Thornton, A. Majumdar, G. Mcadam, Enhanced cerium migration in ceria-stabilised zirconia, Surface and Coatings Technology 94–5 (1–3) (1997) 112–117.
[18] X. Bokhimi, A. Morales, A. Garcia-Ruiz, et al., Transformation of yttrium-doped hydrated zirconium into tetragonal and cubic nanocrystalline zirconia, Journal of Solid State Chemistry 142 (2) (1999) 409–418.
[19] A. Kaiser, A.J. Feighery, D.P. Fagg, Electrical characterization of high titania doped YSZ, Ionics 4 (1998) 215–219.
[20] P. Canton, G. Fagherazzi, R. Frattini, et al., Stabilization of cubic Na-modified $ZrO_2$: a neutron diffraction study, Journal of Applied Crystallography 32 (3) (1999) 475–480.
[21] H.M. Yang, J. Ouyang, X.L. Zhang, et al., Synthesis and optical properties of yttria-doped $ZrO_2$ nanopowders, Journal of Alloys and Compounds 458 (1–2) (2008) 474–478.
[22] R. Milani, R.P. Cardoso, T. Belmonte, et al., Nitriding of yttria-stabilized zirconia in atmospheric pressure microwave plasma, Journal of Materials Research 24 (6) (2009) 2021–2028.
[23] J.P. Markovic, D. Jugovic, M. Mitric, et al., Nanostructured $ZrO_2$ powder synthesized by ultrasonic spray pyrolysis, Surface Review and Letters 14 (5) (2007) 915–919.
[24] V.V. Srdic, M. Winterer, Aluminum-doped zirconia nanopowders: chemical vapor synthesis and structural analysis by rietveld refinement of X-ray diffraction data, Chemistry of Materials 15 (13) (2003) 2668–2674.
[25] Y. Goto, T. Omata, S. Otsuka-Yao-Matsuo, Extremely suppressed grain growth of $Y_2O_3$-stabilized zirconia nanocrystals synthesized by the nonhydrolytic sol–gel technique, Journal of The Electrochemical Society 156 (1) (2009) K4–K9.
[26] Q.H. Zhang, W.G. Fan, L. Gao, Anatase $TiO_2$ nanoparticles immobilized on ZnO tetrapods as a highly efficient and easily recyclable photocatalyst, Applied Catalysis B 76 (1–2) (2007) 168–173.
[27] X.X. Yu, S.W. Liu, J.G. Yu, Superparamagnetic gamma-$Fe_2O_3$@$SiO_2$@$TiO_2$ composite microspheres with superior photocatalytic properties, Applied Catalysis B 104 (1–2) (2011) 12–20.
[28] D.G. Lamas, R.O. Fuentes, I.O. Fábregas, et al., Synchrotron X-ray diffraction study of the tetragonal-cubic phase boundary of nanocrystalline $ZrO_2$–$CeO_2$ synthesized by a gel-combustion process, Journal of Applied Crystallography 38 (6) (2005) 867–873.
[29] S.C. Erwin, L.J. Zu, M.I. Haftel, et al., Doping semiconductor nanocrystals, Nature 436 (7047) (2005) 91–94.
[30] A. Ahniyaz, T. Fujiwara, T. Fujino, et al., Low-temperature direct synthesis of $CeO_2$–$ZrO_2$ solid solution nanoparticles by a hydrothermal method, Journal of Nanoscience and Nanotechnology 4 (3) (2004) 233–238.
[31] X.M. Wang, G. Lorimer, P. Xiao, Solvothermal synthesis and processing of yttria-stabilized zirconia nanopowder, Journal of the American Ceramic Society 88 (4) (2005) 809–816.
[32] K.K. Unger, Porous Silica: Its Properties and Use as Support in Column Liquid Chromatography, Elsevier, Amsterdam, 1979.
[33] F.C. Cebeci, Z.Z. Wu, L. Zhai, et al., Nanoporosity-driven superhydrophilicity: a means to create multifunctional antifogging coatings, Langmuir 22 (6) (2006) 2856–2862.
[34] D.Y. Zhang, P.P. Wang, R.I. Murakami, et al., First-principles simulation and experimental evidence for improvement of transmittance in ZnO films, Progress in Natural Science 21 (1) (2011) 40–45.
[35] H.L. Shen, H. Zhang, L.F. Lu, et al., Preparation and properties of AZO thin films on different substrates, Progress in Natural Science 20 (1) (2010) 44–48.